Supplementary Information (SI) for Journal of Materials Chemistry A.
This journal is © The Royal Society of Chemistry 2026

# Supporting Information

## Synergistic buried interfacial optimization and phase-composition regulation enable highly efficient Dion-Jacobson perovskite solar cells

Liming Jiang,[a] Lunjia Yao,[a] Fengli Zhou,[a] Zhongyi Wen,[a] Hanjun Zhang,[d] Hualin Zheng,[c] Mingfu Ye,[ce] Zhixiang Gao,*[b] Yonghao Zheng,*[a] Xiao Luo,*[a] Dongsheng Wang*[a] and Xiaodong Liu*[abc]

[a]School of Optoelectronic Science and Engineering, University of Electronic Science and Technology of China (UESTC), Chengdu 610054, China.

[b]Shanxi Key Laboratory of Microstructure Electromagnetic Functional Materials, Datong 037000, China.

[c]Optoelectronic Sensor Devices and Systems Key Laboratory of Sichuan Provincial Universities, Chengdu University of Information Technology, Chengdu 610225, China.

[d]School of Pharmacy, Qujing University of Medicine & Health Sciences, Qujing 655100, China.

[e]School of Chemistry and Chemical Engineering, Anhui University of Technology, Maanshan 243002, China.

*Corresponding authors:
E-mail: gao_zhixiang@126.com
E-mail: zhengyonghao@uestc.edu.cn
E-mail: luox@uestc.edu.cn
E-mail: wangds@uestc.edu.cn
E-mail: xdliu@uestc.edu.cn

**Keywords:** Dion-Jacobson phase perovskites, molecular bridge, buried interface passivation, phase composition regulation, solar cells.

**Experimental Section**

**Materials:** 1,4-Diaminobutane diiodide (BDADI) (>99%), lead (II) iodide ($PbI_2$) (9 9.99%) , 4-tert-butylpyridine (tBP), 2,2',7,7'-tetrakis-(N,N-di-pmethoxyphenylamin e)-9,9'-spirobifuorene (Spiro-OMeTAD), lithium bis (trifluoromethylsulfonyl) imide (Li-TFSI), tris(2-(1H-pyrazol-1-yl)-4-tert-butylpyridine)-Cobalt (III) bis(trifluoromethy lsulphonyl)imide (FK209), Formamidinium iodide (FAI) (>99.5), Methylammonium chloride (MACl) (>99.5%) and lead chloride ($PbCl_2$) (>99.5%) were purchased fr om Xi'an Polymer Light Technology Corp. Glycine (Gly) (99.5%) was purchased from Beijing InnoChem Science & Technology Co., Ltd. Ethyl acetate (EA) (>99%) was purchased from Cdkelong, and all other solvents were purchased from Si gma-Aldrich. $SnO_2$ colloid precursor (tin (IV) oxide, 15% in $H_2O$ colloidal disper sion) was purchased from Alfa Aesar. The ITO/glass substrate was obtained fr om Advanced Election Technology Company.

**Preparation of Perovskite Solutions:** (BDA)$FA_4Pb_5I_{16}$ based perovskite precursor solution was prepared by dissolving FAI (0.80 mmol), $PbI_2$ (1.0 mmol), BDADI (0.20 mmol), MACl (0.1 mmol), and $PbCl_2$ (0.1 mmol) in 0.95 mL DMF and 0.05 mL DMSO mixture solvent and stirred at 25°C overnight before using.

**Device Fabrication:** The device structure is ITO/$SnO_2$-Gly/BDA$FA_4Pb_5I_{16}$/Spiro-OMeTAD/ Ag. The detailed experiment processes are as follows: ITO glass substrates were first treated with ultra-sonication in detergent, acetone, isopropanol, and ethanol, followed by UV-ozone for 20 min after drying in $N_2$ stream. Add Gly to the $SnO_2$ nanoparticles colloidal solution (2.5%, diluted with DI water) to prepare a $SnO_2$-Gly solution and stir it overnight. 1 mg/mL $SnO_2$-Gly was spin-coated at 4000 rpm for 30 s on cleaned ITO substrate, then annealing at 180 °C for 20 min. The perovskite solutions were dropped on ITO/ $SnO_2$-Gly substrates and spin-coated at 3000 rpm for 40 s, at the 10th second of the second step, 110 µL of EA was dropped on the rotating substrates. Subsequently, the as-prepared films were thermally annealed at 100 °C for

25 min in a nitrogen atmosphere. The Spiro-OMeTAD solution was prepared by mixing 72.3 mg of Spiro-OMeTAD, 18 µL Li-TFSI/ACN solution (300 mg/mL), 29 µL FK209/ ACN solution (500 mg/1 mL), and 30 µL tBP in 1.1 mL chlorobenzene. And then the Spiro-OMeTAD solutions were spin-coated at 4000 rpm for 30 s. Finally, The Ag electrode (100nm) was thermally evaporated at a rate of 0.4 to 1 Å/s. The active area of the PSCs determined by a shadow mask was 0.04 $cm^2$.

**Film and Device Characterizations:** Dynamic Light Scattering (DLS) measurements were performed on the Malvern Zetasizer Nano ZS90. The X-ray diffraction (XRD) measurements were conducted on a Bruker D8 Advance diffractometer with Cu Kα radiation (λ = 1.5418 Å) and following parameters: 2$\vartheta$ range 5 to 60°, 0.02° step scan, and grazing incidence X-ray diffraction (GIXRD) was measured using a PANalytical X'Pert Powder instrument. Scanning electron microscope (SEM) images were collected using a Gemini SEM 300 electron microscope. X-ray photoelectron spectroscopy (XPS) and ultraviolet photoelectron spectroscopy (UPS) measurements were performed on a Thermo Fisher ESCALAB 250Xi system. UV-vis absorption spectra were acquired on a Shimadzu UV-2600 spectrophotometer. Transient absorption spectroscopy (TAS) was measured with an amplified Ti: sapphire femtosecond laser (800 nm, 50 fs, 1 kHz repetition; Coherent Libra) and a Helios pump/probe setup (Ultrafast Systems). The 405 nm pump pulses with a pump fluence of 0.5 µJ/$cm^2$ were obtained by frequency doubling the 800 nm fundamental regenerative amplifier output. Steady state photoluminescence (PL) spectra and time-resolved photoluminescence (TRPL) spectra were taken on an FLS1000 photoluminescence spectrometer with an excitation wavelength of 405 nm. Photoluminescence quantum yield (PLQY) of perovskite thin films was measured with 405 nm excitation light under the integrating sphere mode (Ocean Optics). In-situ PL spectra were recorded using a QE6500 spectrometer (Ocean Optics) in a nitrogen glovebox under 405 nm excitation light. The current density-voltage (*J-V*) curves of the device were measured under AM 1.5G illumination at 100 mW $cm^{-2}$ (calibrated with a standard Si solar cell) using an Abet Technologies Sun 2000 solar simulator and a Keithley 2400 source meter. The device was measured by voltage

reverse scan (1.6 V to -0.3 V, step 60 mV) and forward scan (-0.3 V to 1.6 V, step 60 mV). External quantum efficiency (EQE) was measured using a QTEST HIFINITY 5 (Crown tech Inc.), and the light intensity was calibrated with standard Si detectors. Transient photocurrent (TPC) measurement was performed with a system excited by a 532 nm (1000 Hz, 3.2 ns) pulse laser. Transient photovoltage (TPV) measurement was performed with the same system excited by a 405 nm (50 Hz, 20 ms) pulse laser.

**DFT calculations:** The quantum chemistry calculations (monomer and simple cluster structures) were carried out with the ORCA 5.0.4 software. The B3LYP functional was adopted for all calculations in combination with the DFT-D3(BJ) dispersion correction. The basis set of def2-SVP was adopted for the geometry optimization and frequency calculations. The geometries were fully optimized without any structural constraints. The frequency calculations were carried out at the same level of theory to verify that all structures have no imaginary frequency. The dipole moment was calculated at the B3LYP-D4/def2-TZVPD level of theory. The electrostatic potential involved in the analyses was evaluated by Multiwfn based on the highly effective algorithm proposed in Ref. The geometric structure figures and ESP figures were rendered by means of the VMD visualization program. The first principal calculations (periodicity structures) were carried out with the CP2K 2024.1 software package with Perdew-Burke-Ernzerhof (PBE) functional and Grimme's D3 van der Waals correction method, during which the DZVP-MOLOPT-SR-GTH basis set and Goedecker-Teter-Hutter (GTH) pseudopotential were employed. The single point energy was calculated with the TZVP-MOLOPT-GTH and TZVP-MOLOPT-SR-GTH basis set. To steer clear of the interactions between periodic images, the vacuum layers larger than 20 Å were added to non-periodic directions. The plane-waves were cut off at 400 Ry. The geometric structure figures and difference map for electron density were rendered by means of VESTA visualization program. The adsorption energy ($E_{ads}$) of adsorbate molecule was defined as: $E_{ads} = E_{mol}/surf\text{-}E_{surf}\text{-}E_{mol}(g)$. where $E_{mol}/surf$, $E_{surf}$ and $E_{mol}(g)$ are the energy of adsorbate molecule adsorbed on the surface, the energy of clean surface, and the energy of isolated molecule in a cubic periodic box, respectively.

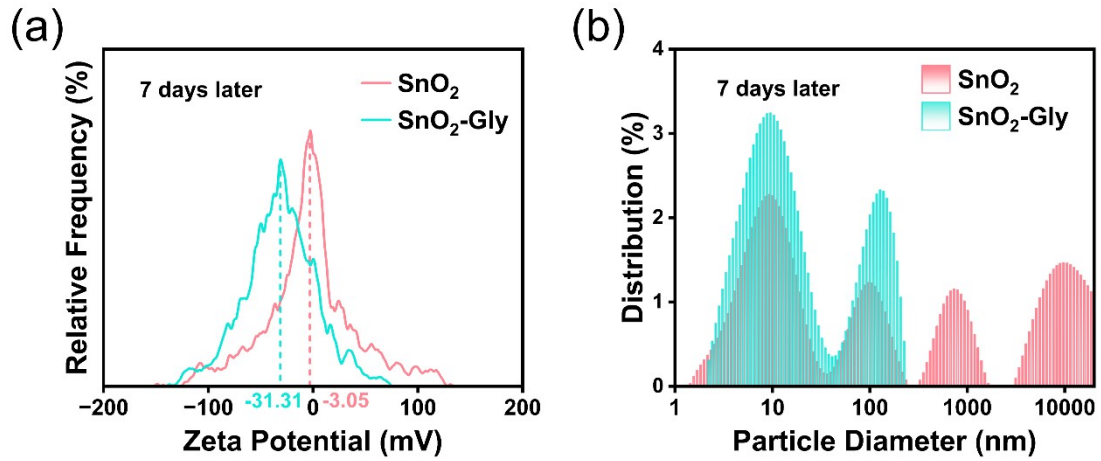


**Fig. S1** (a) The Zeta potential and (b) DLS particle size distribution of $SnO_2$ and $SnO_2$-Gly after 7 days of aging.

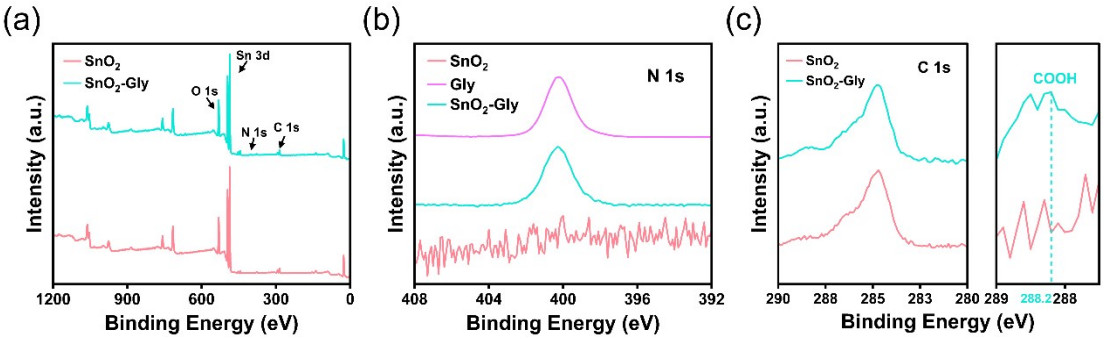


**Fig. S2** XPS spectra of $SnO_2$ and $SnO_2$-Gly. (a) Survey spectra (b) N 1s spectra. (c) C 1s spectra.

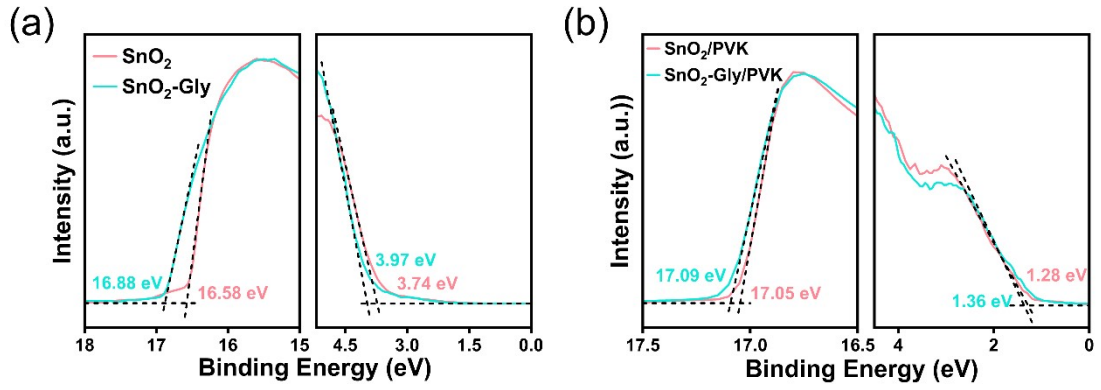


**Fig. S3** UPS spectra showing the $E_{cut\text{-}off}$ and $E_{on\text{-}set}$ binding energies of (a) $SnO_2$ and $SnO_2$-Gly, and (b) $SnO_2$/PVK and $SnO_2$-Gly/PVK.

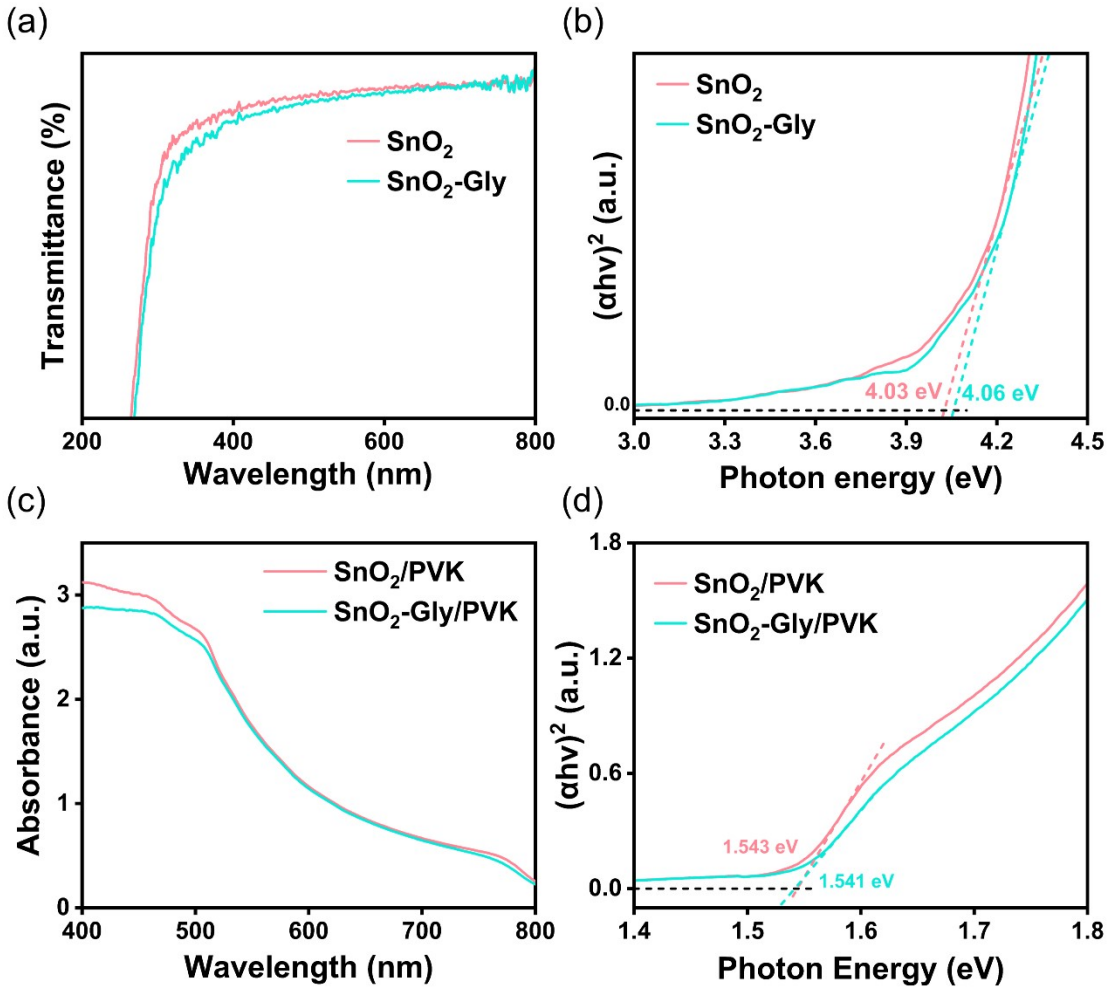


**Fig. S4** (a) UV transmission spectra of $SnO_2$ and $SnO_2$-Gly. (b) Tauc plots of $SnO_2$ and $SnO_2$-Gly. (c) UV-vis absorption spectra of perovskite films deposited on $SnO_2$ and $SnO_2$-Gly. (d) Tauc plots of the corresponding perovskite films.

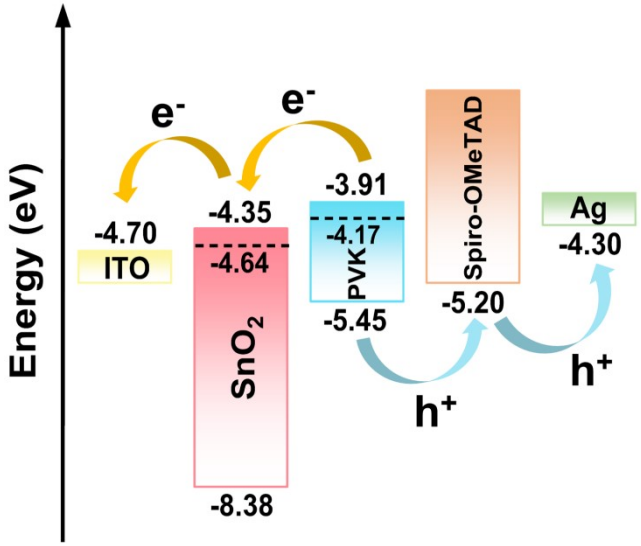


**Fig. S5** Energy-level diagram of the functional layers in the PSC device based on pristine $SnO_2$ and $SnO_2$/PVK films.

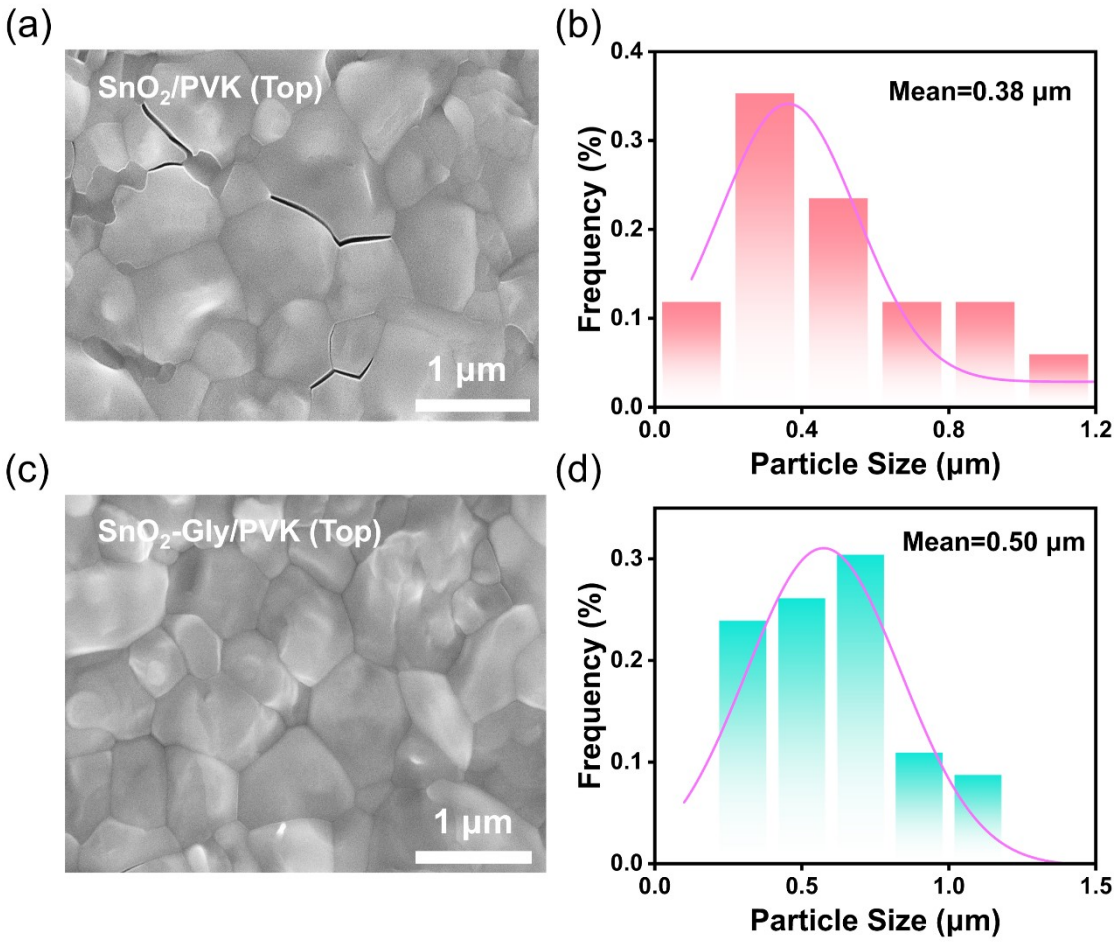


**Fig. S6** (a, c) SEM image of the perovskite film. (b, d) Particle size distribution of the perovskite film.

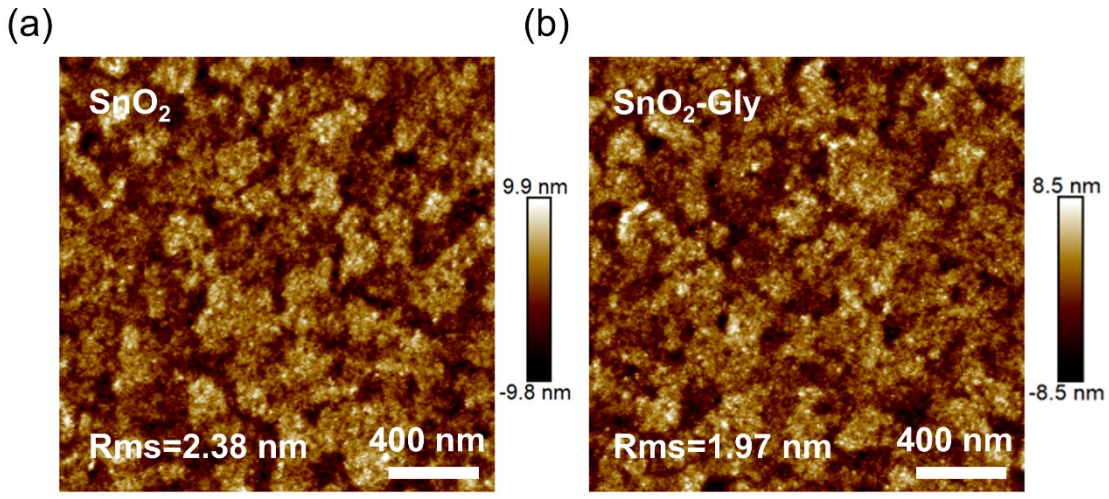


**Fig. S7** The AFM images of (a) $SnO_2$ and (b) $SnO_2$-Gly films.

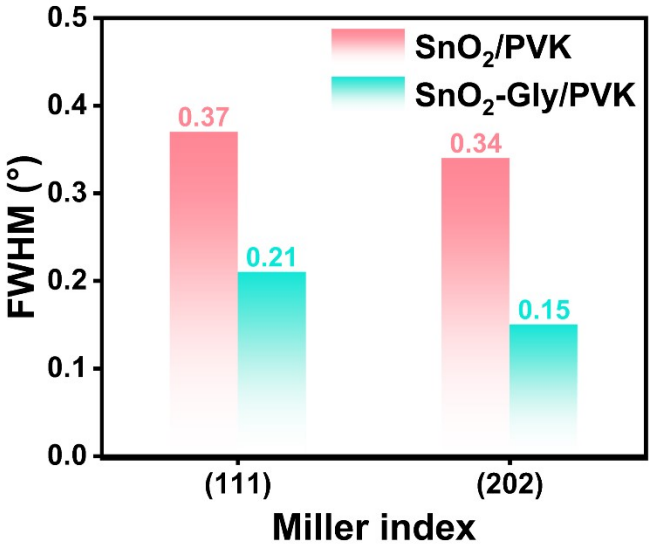


**Fig. S8** The FWHM of the (111) and (202) crystal plane of $SnO_2$/PVK and $SnO_2$-Gly/PVK films by XRD.


**Fig. S9** The DMF contact angles on the surfaces of (a) $SnO_2$ and (b) $SnO_2$-Gly films.

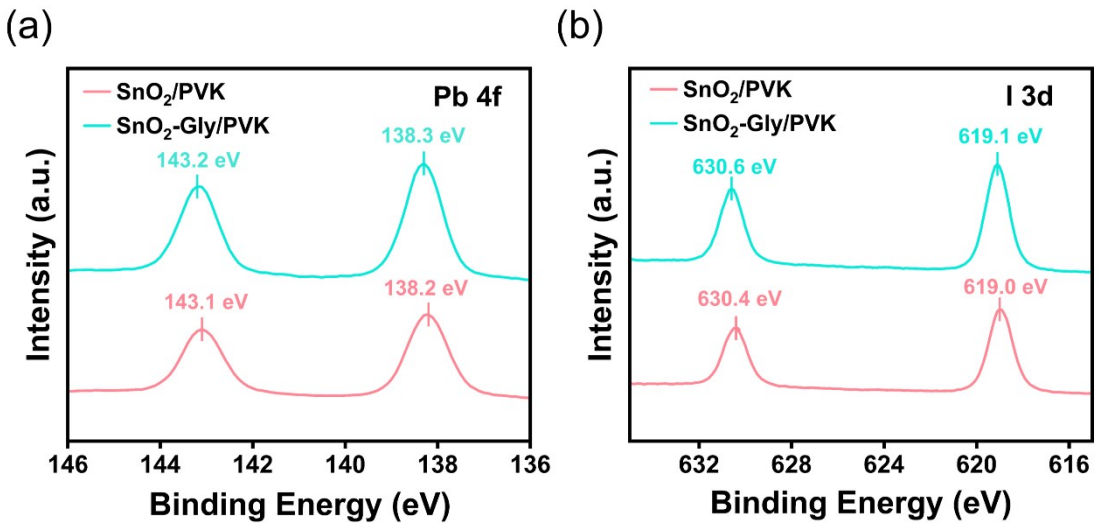


**Fig. S10** The XPS spectra of $SnO_2$/PVK and $SnO_2$-Gly/PVK (a) Pb 4f, (b) I 3d

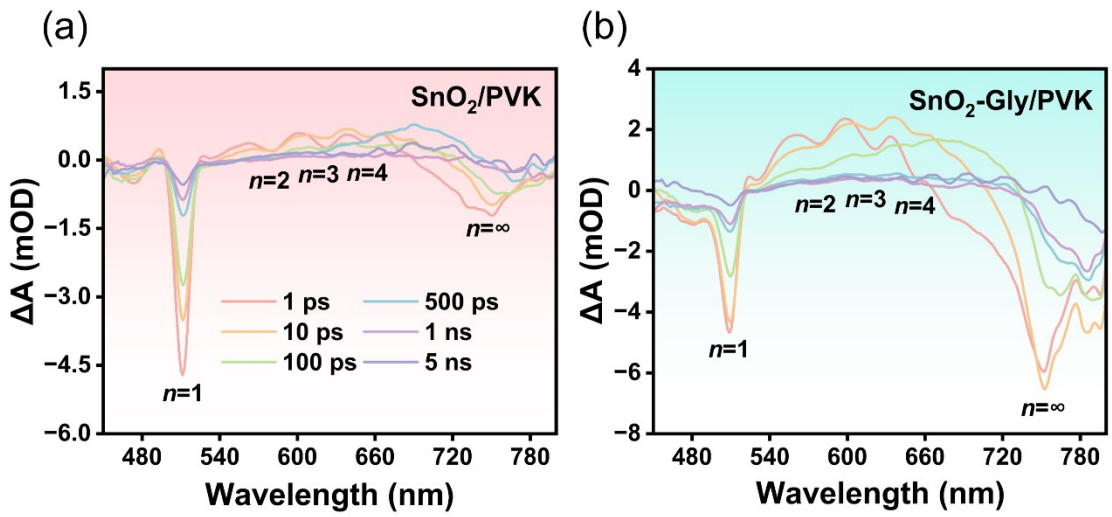


**Fig. S11** TA spectra measured (a) $SnO_2$/PVK, and (b) $SnO_2$-Gly/PVK from the glass side.

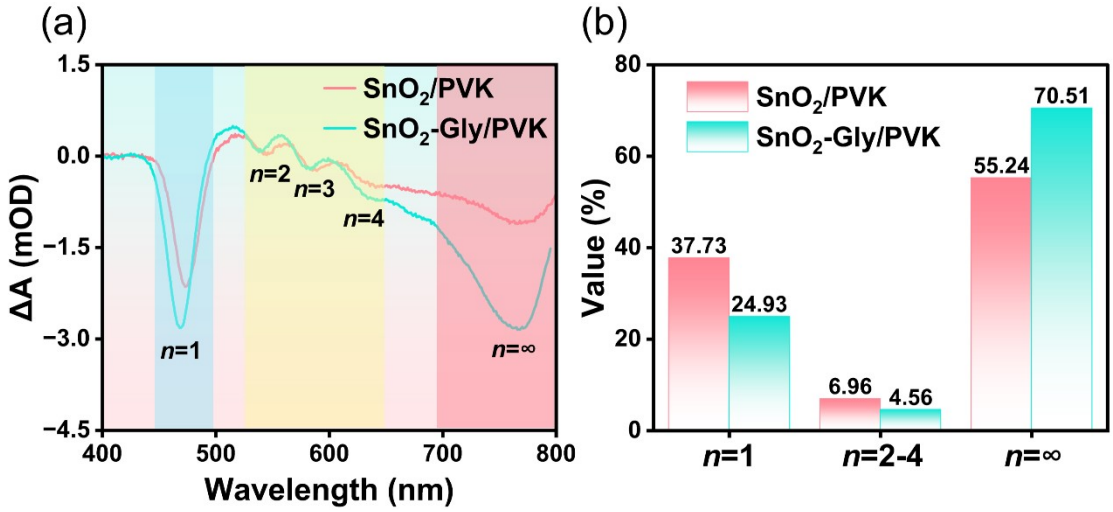


**Fig. S12** (a) TA spectrogram of the perovskite film at 1 ps time. (b) Statistical graph of the PB peak areas of the perovskite film in different n phases.

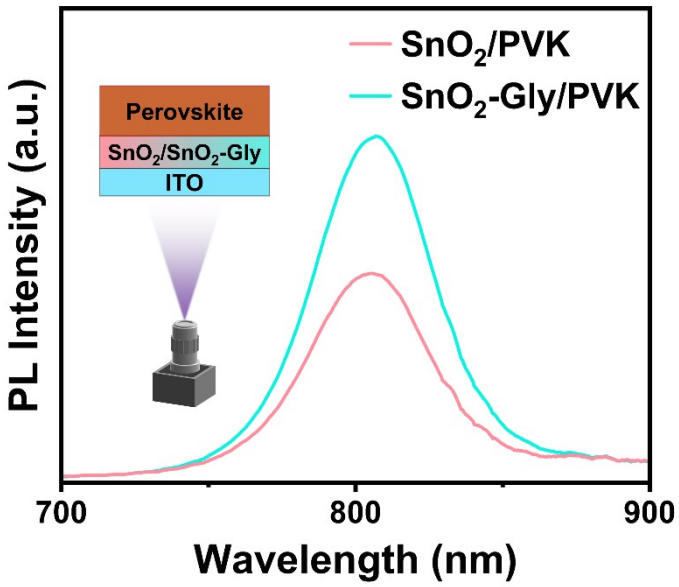


**Fig. S13** Steady-state PL spectra of $SnO_2$/PVK and $SnO_2$-Gly/PVK films with the excitation direction from the glass side.

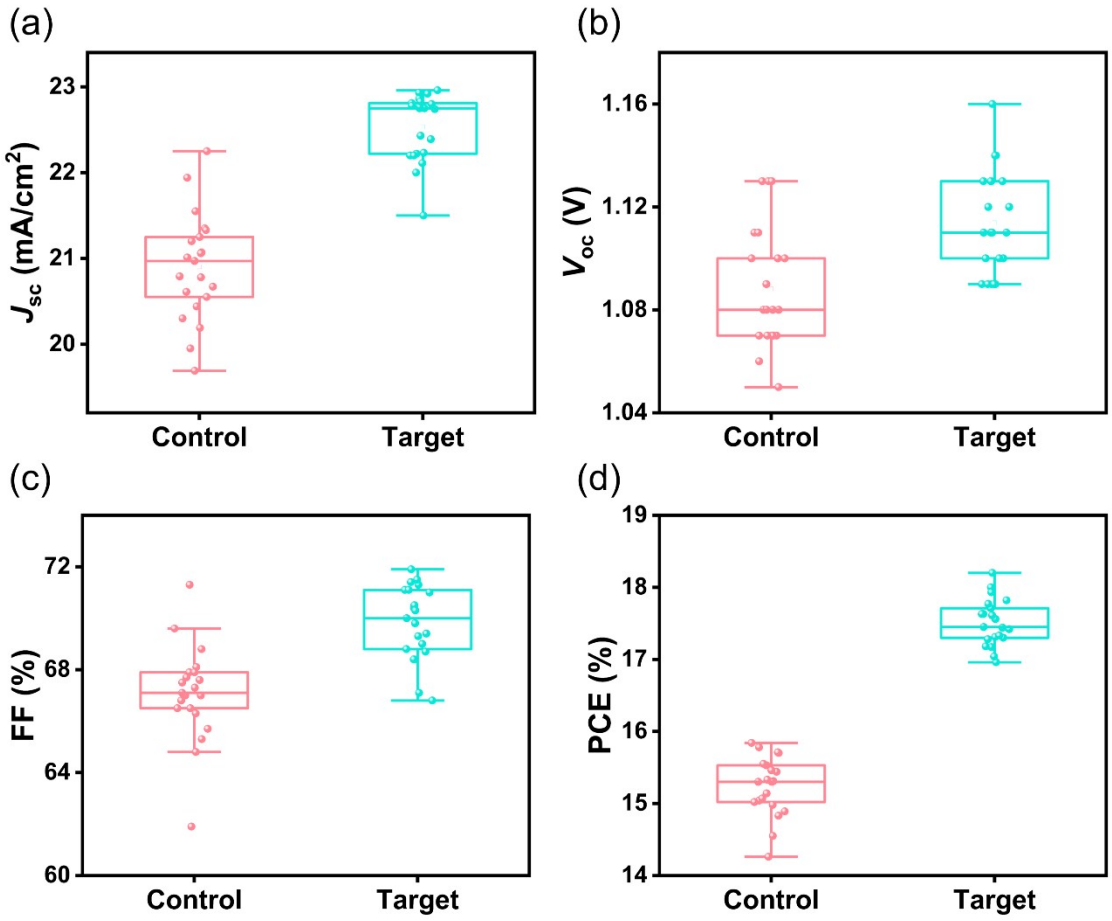


**Fig. S14** The statistics of Q-2D PSCs devices. (a) $J_{sc}$. (b) $V_{oc}$. (c) FF. (d) PCE.

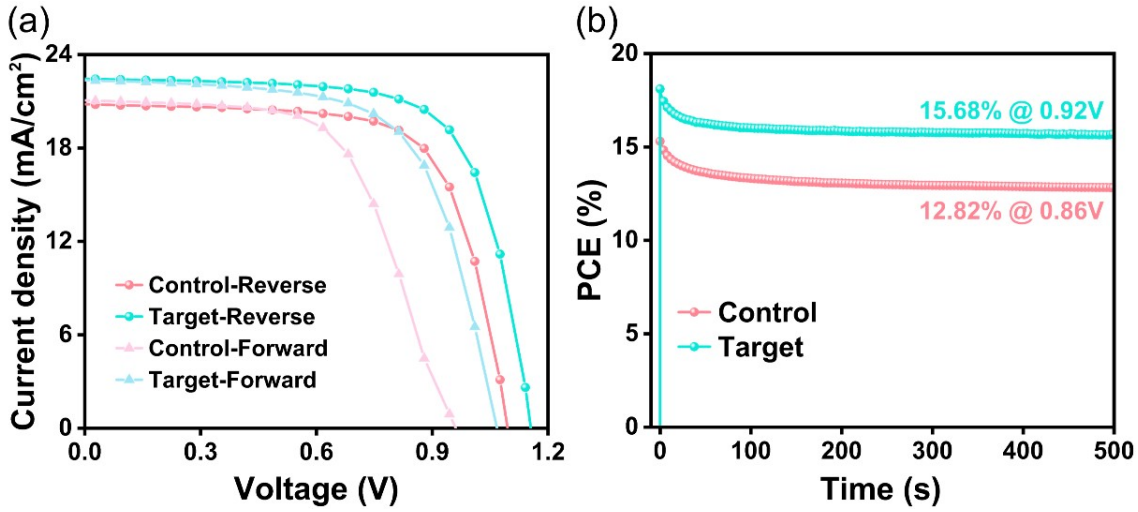


**Fig. S15** (a) Forward and reverse scan *J-V* diagrams of Q-2D PSCs, (b) Stabilized power output at the maximum power point as a function of time.

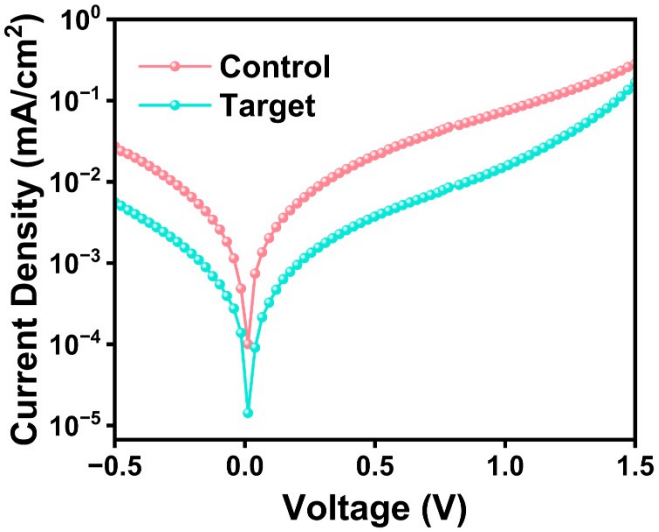


**Fig. S16** Dark *J-V* curves of Q-2D PSCs.

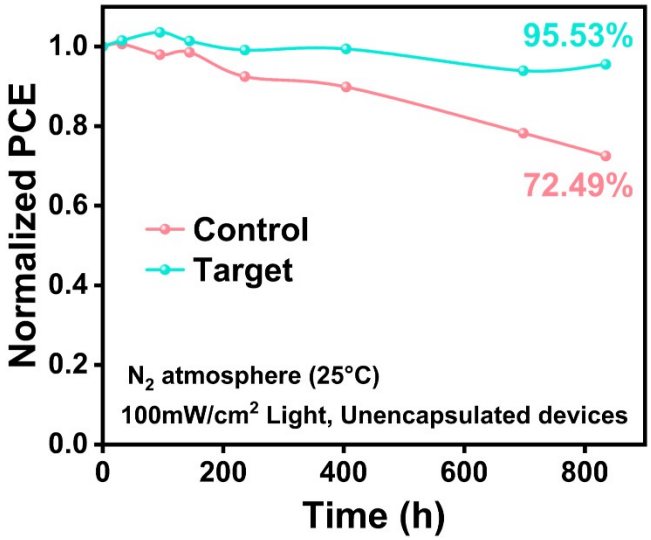


**Fig. S17** Long-term stability test for unencapsulated PSCs under continuous LED light irradiation at 100 mW $cm^{-2}$(ISOS-L-1 Protocol).

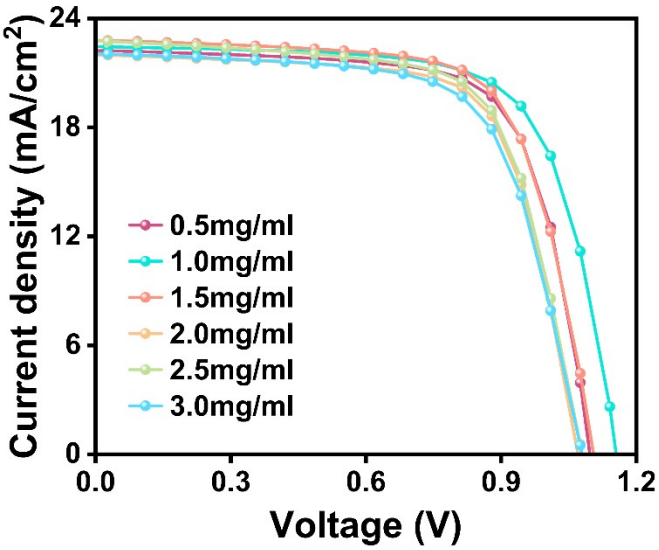


**Fig. S18** *J-V* curves of the PSCs based on $SnO_2$-Gly ETLs with different Gly doping concentrations.

**Table S1.** Fitting components from TA kinetics of $SnO_2$/PVK and $SnO_2$-Gly/PVK films.

| Phase | Samples | $A_d$ | $\tau_d$ | $A_g$ | $\tau_g$ |
|---|---|---|---|---|---|
| n=1 | $SnO_2$/PVK | 0.94 | 0.54 | / | / |
| n=1 | $SnO_2$-Gly/PVK | 0.97 | 1.05 | / | / |
| n=∞ | $SnO_2$/PVK | / | / | 1.20 | 0.96 |
| n=∞ | $SnO_2$-Gly/PVK | / | / | 1.25 | 0.90 |

The kinetics extracted from TA spectra are fitted with Exponential Growth Decay function:

$$I(t) = \begin{cases} I_0 + A_d + A_g\left(e^{-t_c/\tau_g} - e^{-t/\tau_g}\right), & t \le t_c \\ I_0 + A_d e^{-(t-t_c)/\tau_d}, & t > t_c \end{cases}$$

where $t$ is the pump–probe delay time and $I(t)$ represents the transient absorption signal intensity at a given delay, $I_0$ is the baseline offset of the TA signal, $A_g$ is the growth amplitude, $\tau g$ is the growth time, $t_c$ is the crossover time, $A_d$ is the decay amplitude separating the growth-dominated regime from the decay-dominated regime, $\tau d$ is the decay time.

**Table S2.** Fitting parameters of TRPL spectra of $SnO_2$/PVK and $SnO_2$-Gly/PVK films.

| Samples | $A_1$ | $\tau_1$ (ns) | $A_2$ | $\tau_2$ (ns) | $A_3$ | $\tau_3$ (ns) | $\tau_{avg}$ (ns) |
|---|---|---|---|---|---|---|---|
| $SnO_2$/PVK | 0.59 | 158.46 | 2.84 | 44.96 | 0.018 | 1698.55 | 287.89 |
| $SnO_2$-Gly/PVK | 0.49 | 164.74 | 2.49 | 54.04 | 0.02 | 1933.92 | 365.32 |

**Table S3.** Photovoltaic parameters of Control and Target PSCs.

| Samples | Scanning direction | $J_{sc}$ (mA/cm$^2$) | $V_{oc}$ （V） | FF (%) | PCE (%) | HI (%) |
|---|---|---|---|---|---|---|
| Control | R | 20.79 | 1.10 | 69.6 | 15.84 | 23.61 |
| Control | F | 21.05 | 0.96 | 59.8 | 12.10 | |
| Target | R | 22.43 | 1.16 | 70.3 | 18.20 | 14.84 |
| Target | F | 22.33 | 1.07 | 65.0 | 15.50 | |

**Table S4.** Photovoltaic parameters of the PSCs based on $SnO_2$-Gly ETLs with different Gly doping concentrations.

| Concentration （mg/ml） | $V_{OC}$ (V) | $J_{SC}$ (mA/cm$^2$) | FF (%) | PCE (%) |
|---|---|---|---|---|
| 0.5 | 1.10 | 22.20 | 71.1 | 17.32 |
| 1.0 | 1.16 | 22.43 | 70.3 | 18.20 |
| 1.5 | 1.11 | 22.78 | 70.0 | 17.62 |
| 2.0 | 1.07 | 21.97 | 70.5 | 16.59 |
| 2.5 | 1.08 | 22.75 | 68.6 | 16.85 |
| 3.0 | 1.08 | 22.03 | 67.6 | 16.07 |